Electronic Supplementary Information for Amphoteric Doping in $CuInTe_2$

Vanessa Meschke,[†] Angela Pak,[‡] Jesse M. Adamczyk,[†] Lídia C. Gomes,[‡] Samantha M. Baumann,[¶] Grace A. Rome,[¶] Claire Porter,[†] Kamil Ciesielski,[†] Elif Ertekin,[‡] and Eric S. Toberer*[,†]

†*Department of Physics, Colorado School of Mines, Golden, CO, USA*

‡*Department of Mechanical Science and Engineering, University of Illinois Urbana Champaign, Champaign, IL USA*

¶*Department of Materials and Metallurgical Engineering, Colorado School of Mines, Golden, CO USA*

E-mail: etoberer@mines.edu

SEM Images and X-ray Diffraction Patterns

The following figures show SEM images and the x-ray diffraction (XRD) patterns of the pellets studied in this work. The XRD patterns are referenced to the chalcopyrite structured $CuInTe_2$ (space group 122, $I\bar{4}2d$) from Collection Code 73352 in the Inorganic Crystal Structures Database.

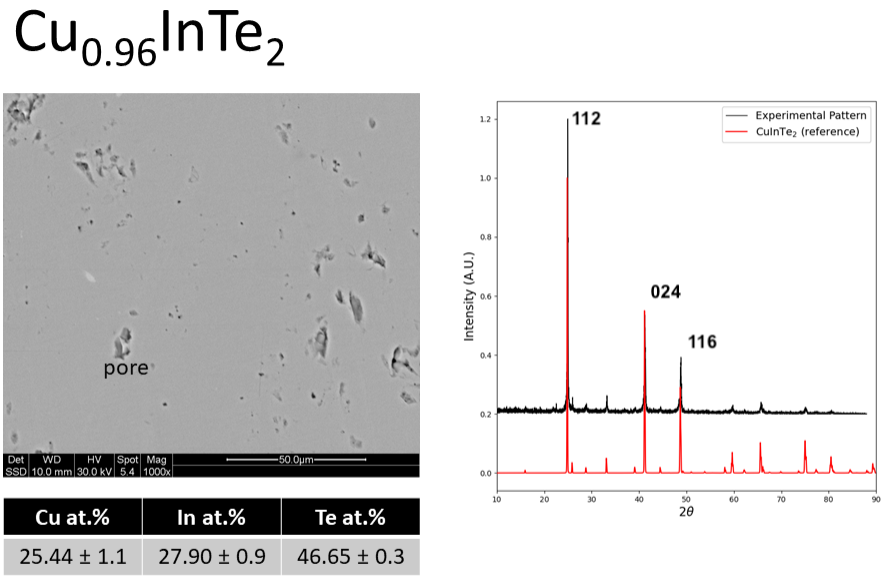

Figure S1: SEM image showing high density microstructure and single phase behavior. The low fraction of pores will not significantly impact transport behavior. XRD shows only the $CuInTe_2$ phase. Te concentration in the EDS measurements is low as a result of instrumental error.

$Cu_{0.96}InTe_2Zn_{0.04}$

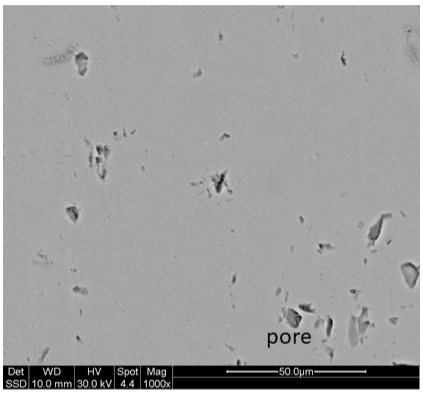

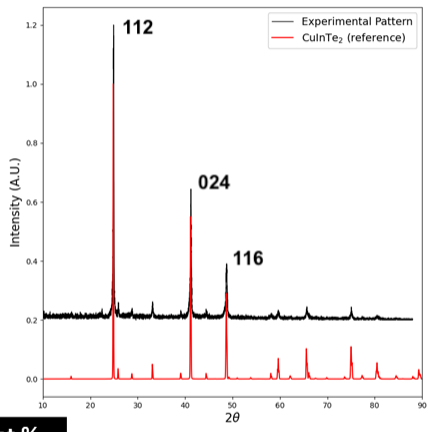

Cu at.%	In at.%	Te at.%	Zn at.%
25.13 ± 0.7	26.95 ± 0.4	46.03 ± 0.9	1.89 ± 1.0

Figure S2: Zn doped $CuInTe_2$ showing single phase behavior in both SEM and XRD. Porosity will only have a minimal effect on the electronic transport properties.

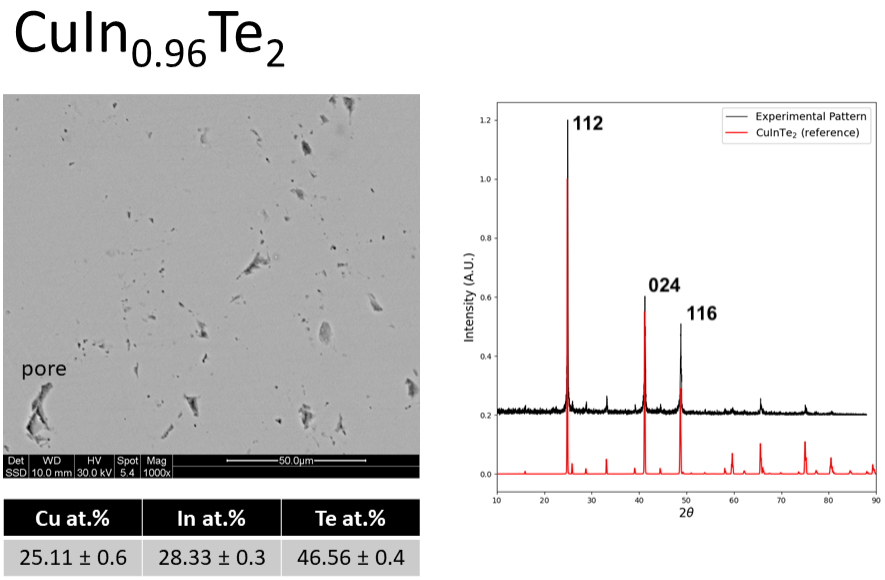

Cu at.%	In at.%	Te at.%
25.11 ± 0.6	28.33 ± 0.3	46.56 ± 0.4

Figure S3: Zn doped $CuInTe_2$ showing single phase SEM and XRD behavior.

$CuIn_{0.96}Te_2Zn_{0.04}$

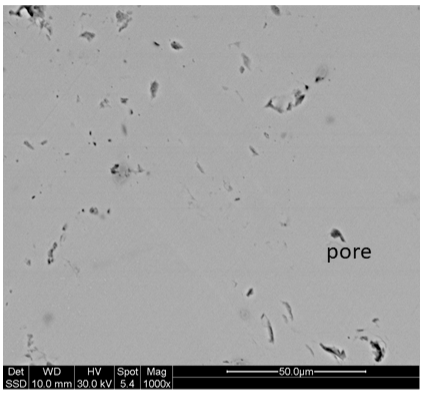

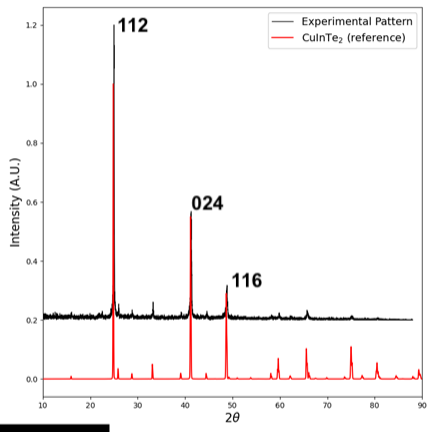

Cu at.%	In at.%	Te at.%	Zn at.%
24.39 ± 0.3	27.10 ± 0.7	46.64 ± 0.2	1.86 ± 0.5

Figure S4: Zn doped $CuInTe_2$ showing minor porosity and single phase behavior.

Table S1: Lattice parameters of native and doped $CuInTe_2$ from Rietveld refinements. Average grain sizes are relatively large and will not have a major effect on electronic transport.

Sample Composition	**a (Å)**	**c (Å)**	**Average Grain Size (μm)**
$Cu_{0.96}InTe_2$	6.211905	12.358688	43
$Cu_{0.96}InTe_2Zn_{0.04}$	6.22055	12.355338	24
$CuIn_{0.96}Te_2$	6.218583	12.404658	39
$CuIn_{0.96}Te_2Zn_{0.04}$	6.215596	12.397016	27

Speed of Sound

Table S2: Longitudinal and shear speed of sound of native and doped $CuInTe_2$.

Sample Composition	**Longitudinal (m/s)**	**Shear (m/s)**
$Cu_{0.96}InTe_2$	3531	1826
$Cu_{0.96}InTe_2Zn_{0.04}$	3561	1845
$CuIn_{0.96}Te_2$	3334	1789
$CuIn_{0.96}Te_2Zn_{0.04}$	3501	1835

Selection of Zn chemical potential

Selection of the chemical potential and synthesis temperature for the CIT space is a delicate process given the sensitivity of the system to perturbations in defect concentrations. In this case, we can see that a $\Delta\mu_{Zn}$ = -1.38 eV/atom and T_{synth} = 623 K matches for point CT2 well (expected carrier concentrations of 1×10^{19} and 5×10^{19} cm^{-3} for the undoped and doped cases, respectively, shown with the horizontal dashed yellow lines). For point IT1, $\Delta\mu_{Zn}$ = -1.25 eV/atom and T_{synth} = 623 K matches the experimental data well (expected carrier concentrations of 3×10^{19} and 4×10^{15} cm^{-3} for the undoped and doped cases, respectively, shown in the horizontal, navy dashed lines).

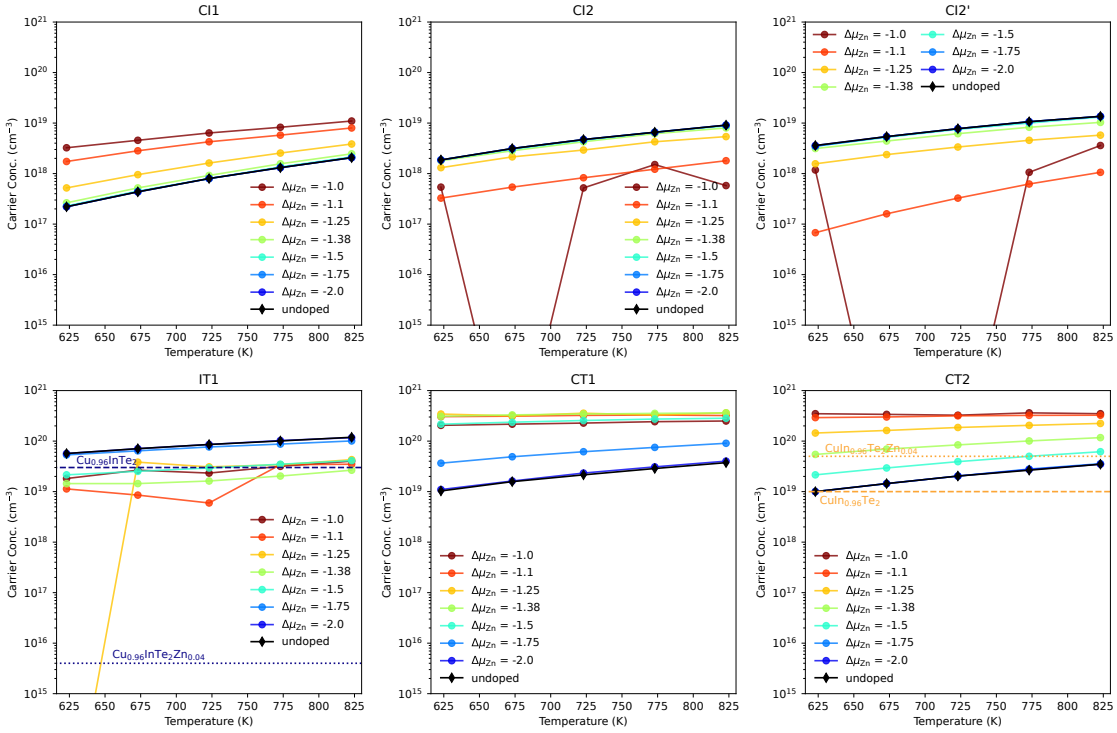

Figure S5: For each invariant point from the original phase equilibria space, the measured carrier concentrations at 323 K is highly sensitive to the chemical potential of Zn (color) as well as synthetic temperature (x-axis).

Defect diagrams

Undoped Defect Diagrams

The defect diagrams for the undoped samples are shown below. The summary of these diagrams is shown in the main text in the Brouwer diagram. A synthetic temperature of 623 K was selected for these diagrams.

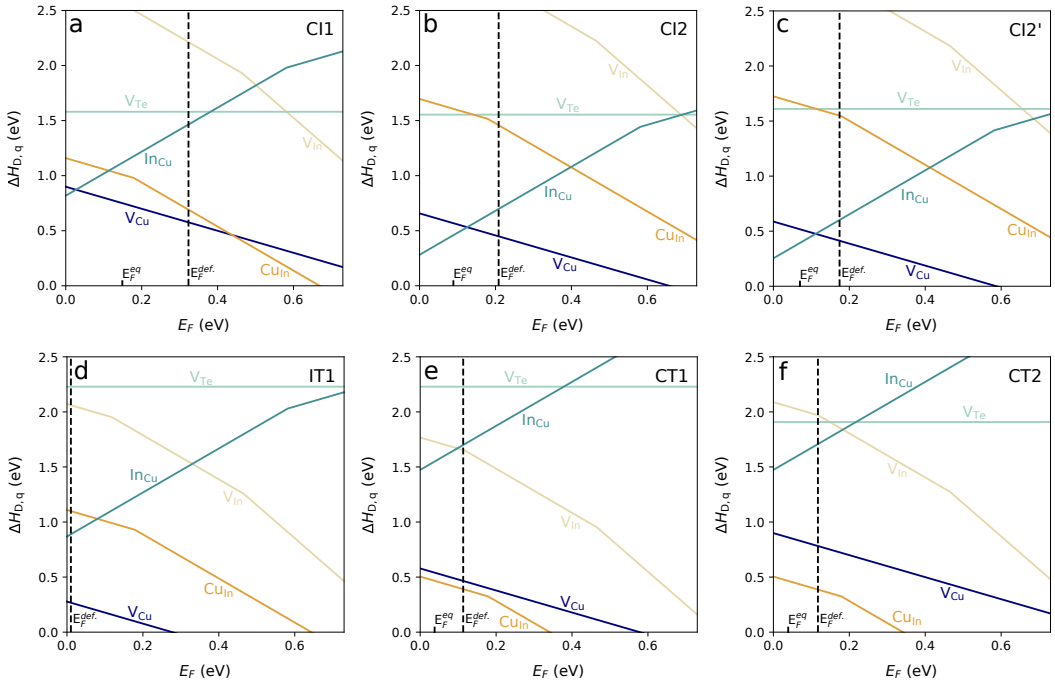

Figure S6: Defect diagrams for native defects in $CuInTe_2$ corresponding to the six invariant points (three-phase equilibrium points) in chemical potential space.

Doped Defect Diagrams

Defect diagrams for varying levels of $\Delta\mu_{\mathrm{Zn}}$ are shown for the chemical potentials that were chosen by assessing the curves in S5.

$\Delta\mu_{\mathrm{Zn}}$ = **-1.25 eV/atom**

Defect diagrams for doped $CuInTe_2$ doped with Zn for a chemical potential $\Delta\mu_{\mathrm{Zn}}$ = -1.25 eV/atom and a synthetic temperature of 623 K. The Fermi level at synthesis (E_F^{def}) and at measurement temperature (E_F^{eq}) are inside the valence band for points CT1 and CT2. CT1 has E_F^{def} = -0.16 eV and E_F^{eq} = -0.18 eV, and CT2 has E_F^{def} = -0.06 eV and E_F^{eq} = -0.08 eV.

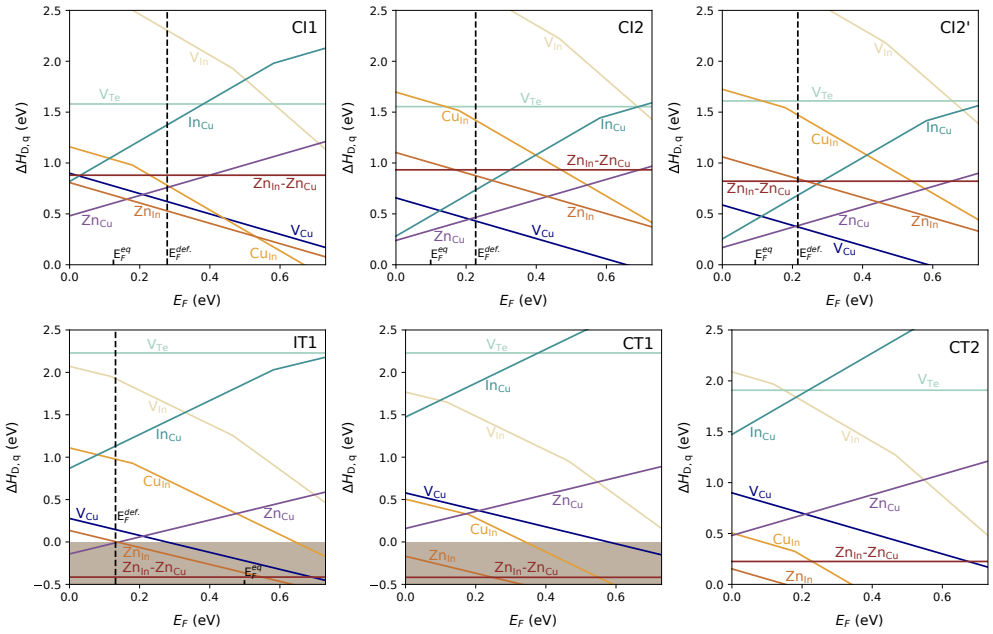

Figure S7: Defect diagrams for defects in $CuInTe_2$ doped with Zn corresponding to the six invariant points (three-phase equilibrium points) in chemical potential space. These plots are shown for $\Delta\mu_{\mathrm{Zn}}$ = -1.25 eV/atom and $T_{synth.}$ = 623 K.

$\Delta\mu_{Zn}$ = **-1.38 eV/atom**

For point CT2, a synthetic temperature of 623 K and a $\Delta\mu_{Zn}$ = -1.38 eV/atom best matched the experimental data. The Brouwer band diagram and defect diagrams are shown for these conditions below.

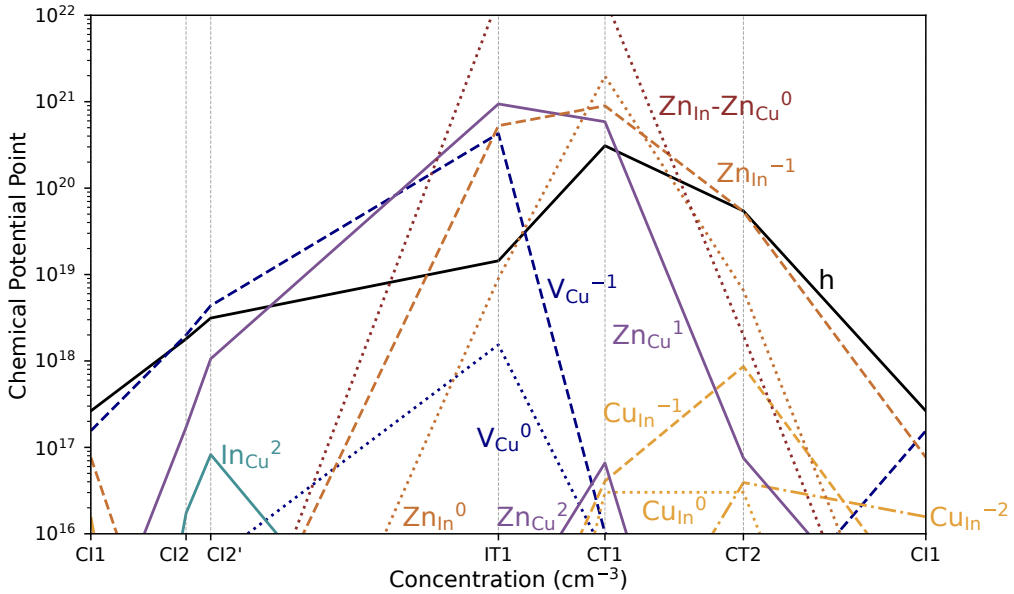

Figure S8: Brouwer diagram for Zn-doped $CuInTe_2$ at $\Delta\mu_{Zn}$ = -1.38 eV/atom and T_{synth} = 623 K.

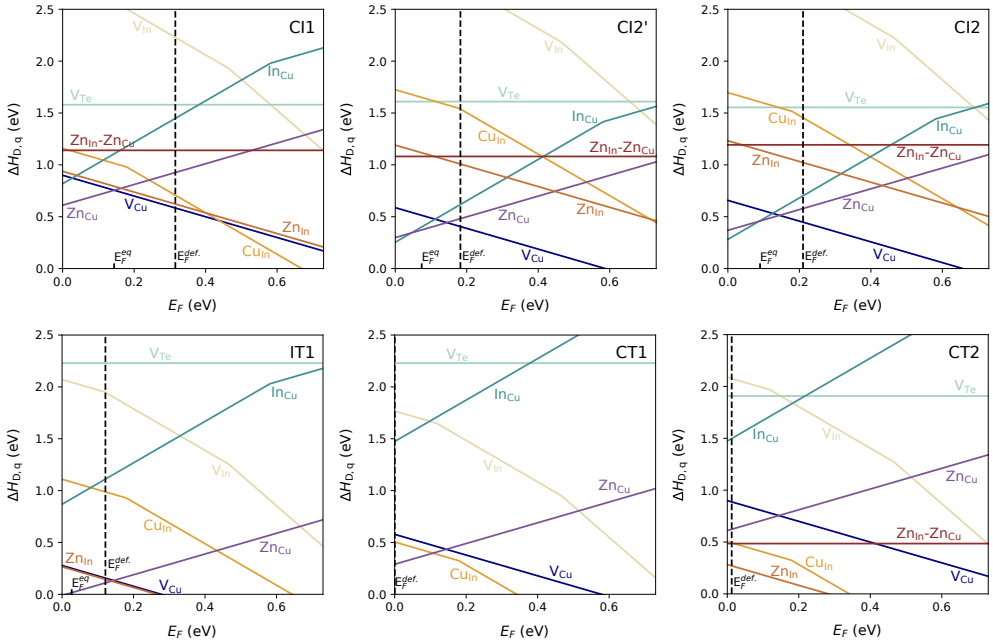

Figure S9: Defect diagram for defects in $CuInTe_2$ doped with Zn with $\Delta\mu_{Zn}$ = -1.38 eV/atom and T_{synth} = 623 K.

Table S3: Three-phase equilibrium points predicted from DFT calculations for $CuInTe_2$ doped with Zn.

Invariant point	$\Delta\mu_{Cu}$	$\Delta\mu_{In}$	$\Delta\mu_{Te}$	**Phases**
CI1	0	-0.438	-0.649	Cu, $Cu_{11}In_9$
CI2	-0.242	-0.143	-0.675	$Cu_{11}In_9$, In_4Te_3
CI2'	-0.312	-0.185	-0.619	In_4Te_3, $CuIn_5Te_8$
IT1	-0.622	-1.11	0	$CuIn_5Te_8$, Te
CT1	-0.321	-1.414	0	Te, CuTe
CT2	0	-1.093	-0.321	CuTe, Cu

zT

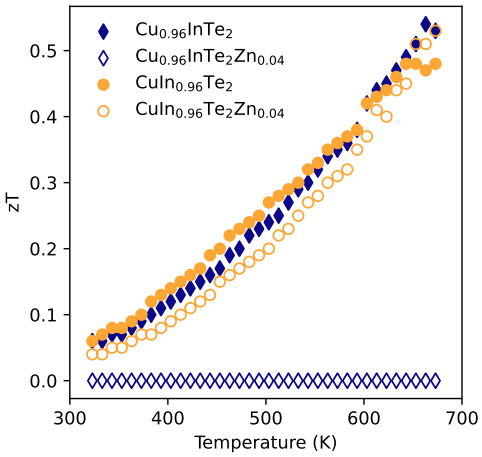

Figure S10: Thermoelectric figure of merit (zT) shows little variation in the majority of the samples studied in this work. However, the Zn-doped copper-deficient sample shows poor zT due to its low carrier concentration.

Total Thermal Conductivity

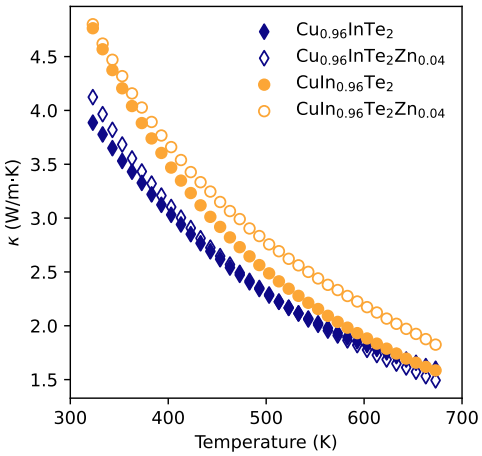

Figure S11: Total thermal conductivity measurements closely follow the κ_l data presented in the main text, indicating minimal electronic contributions to the overall thermal conductivity.